J. Fluid Mech. (2006), *vol.* 547, *pp.* 215–230.
doi:10.1017/S0022112005007354 Printed in the United Kingdom

Chaotic streamlines in a translating drop with a uniform electric field

By THOMAS WARD† AND G. M. HOMSY

Department of Mechanical and Environmental Engineering, University of California, Santa Barbara, CA 93106, USA

(Received 8 September 2003 and in revised form 29 June 2005)

A drop translating in the presence of a uniform electric field is studied both theoretically and experimentally to determine qualitative properties of three-dimensional chaotic particle trajectories and mixing in bounded Stokes flows. The flow is a combination of a Hadamard–Rybczynski and a Taylor circulation due to the translation and electric field respectively. The three-dimensional trajectories are generated by tilting the electric field relative to the drop translational motion by an angle α. The numerical analysis includes qualitative analysis of the degree of mixing by Poincaré mapping, quantitative estimates of the largest mixed volume fraction and the rate of mixing characterized by the largest Lyapunov exponent. Experiments are performed using a castor oil/silicone oil system for the continuous and dispersed phases respectively. Single trajectories are studied by visualizing small neutrally buoyant glass particles inside the dispersed phase using a stereoscopic particle tracking technique. Drops are approximately 5 mm in diameter, settling velocities are $O(0.1\,\mathrm{mm\,s^{-1}})$ and the electric fields are $O(10\,\mathrm{V\,mm^{-1}})$. We observe crossings of the unperturbed separatrix and particle trajectories that show evidence of a symmetry plane, both important features of the theory.

1. Introduction

Bajer & Moffatt (1990) were apparently the first to consider the possibility that steady three-dimensional flows inside drops could contain chaotic streamlines. They treated general bounded quadratic flows and showed that such flows could exhibit 'stretch–twist–fold' kinematics, leading to chaotic advection. Lyapunov exponents for bounded flows were first computed by Bajer, Moffatt & Nex (1990) and the effects of inertia were considered by Bajer & Moffatt (1992). Stone and coworkers analysed numerically the possibility of chaotic advection in a steady three-dimensional Stokes flow. Kroujiline & Stone (1999) considered two possible three-dimensional internal velocity fields. The first consisted of a drop translating due to buoyancy forces and the second a drop in an extensional flow, first introduced in Stone, Nadim & Strogatz 1991. The addition of a vorticity vector that is not aligned with the axis of each of these velocity fields produced stedy three-dimensional chaotic streamlines. The mixing was studied computationally through the dependence of Poincaré maps on the parameters. More recently Stone & Stone (2005) analytically studied mixing inside

† Present address: Division of Engineering and Applied Sciences, Harvard University, 29 Oxford Street, Cambridge, MA 02138-2901, USA. tward@deas.harvard.edu.

of droplets in curved microchannels where the velocity field is a combination of buoyancy-driven and shear flow.

Bryden & Brenner (1999) considered enhancement of mass transfer inside a drop by chaotic advection in a steady three-dimensional Stokes flow. Their problem consists of a drop translating due to buoyancy subjected to a shear flow. The parameters include the angle between the velocity and vorticity vectors, the viscosity ratio and a dimensionless shear rate. Their analysis includes visualization of the mixed regions through Poincaré maps and calculating the mass transfer coefficients by solving the convection–diffusion equation at finite Péclet and Sherwood numbers. The mass transfer coefficients for $Pe > 1$, for pure shear and pure translation, indicated diffusion-limited transport, in general agreement with the classical work of Kronig & Brink (1949). However the mass transfer rates become convection dominated in the parameter regime in which chaotic streamlines nearly fill the drop.

A remarkable property, observed by and commented upon by all these authors, is that small perturbations from axisymmetry can lead to a chaotic domain of size $O(1)$ in bounded laminar flows. Vainshtein, Vasiliev & Neishtadt (1996) and Neishtadt, Vainshtein & Vasiliev (1998) have developed an analytical understanding of this phenomenon using a perturbation technique. The approach considers small $O(\epsilon)$ perturbations, where $\epsilon \ll 1$, to what would otherwise be an integrable system. The key idea is that the system will spend most of its time near a closed streamline of the unperturbed system and that one can identify variables that are invariant along such a streamline. The system exhibits only a slow drift in the value of the adiabatic invariant (Cary, Escande & Tennyson 1986) until a trajectory crosses a separatrix of the unperturbed flow (denoted hereafter as the SUF) during which the adiabatic invariant undergoes an $O(1)$ jump in its value. To compute these jumps, the three-dimensional equations of motion are averaged by separating the motion into fast and slow variables (Neishtadt 1984). The motions are averaged over the fast variable yielding an averaged system that resembles a Hamiltonian with a conserved quantity Φ, that is the adiabatic invariant of the exact system (Neishtadt *et al.* 1996, 1998). The change in Φ is analysed by expanding the adiabatic invariant, Φ, in an $O(\epsilon)$ region near the SUF similar to boundary layer analysis. The highest-order term in the expansion determines the magnitude of the jump to an accuracy of $O(\epsilon)$. In two separate studies (Neishtadt *et al.* 1996, 1998) the technique is applied to the flow situations studied by Bajer & Moffatt (1990) and by Stone *et al.* (1991). For example, in the latter case the unperturbed flow is the axisymmetric quadrupole circulation and the perturbation is the addition of a slightly tilted rotation in the drop. The predictions of the semi-analytical perturbation technique are in good agreement with numerical solutions of the full three-dimensional advection equations of motion. The results show that even a small tilt of $O(\epsilon)$ can produce $O(1)$ regions of mixing due to multiple crossings of the SUF.

In this paper we consider a translating drop in the presence of a spatially uniform electric field. The drop and surrounding fluid are viscous and non-conducting and the drop is assumed to remain spherical. The internal circulation produced by the translational motion is the Hadamard–Rybczynski circulation shown in figure 1(*a*). The circulation produced by the uniform electric field is commonly referred to as the Taylor circulation and is shown in figure 1(*b*) (Taylor 1966). Both of these circulations are axisymmetric so if their axes are parallel, the resulting flow is axisymmetric with closed streamlines (Chang, Carleson & Berg 1981). If instead we consider the case where the axes are not parallel, the resulting flow field is three-dimensional and some streamlines may fill the entire interior of the drop, although for this specific

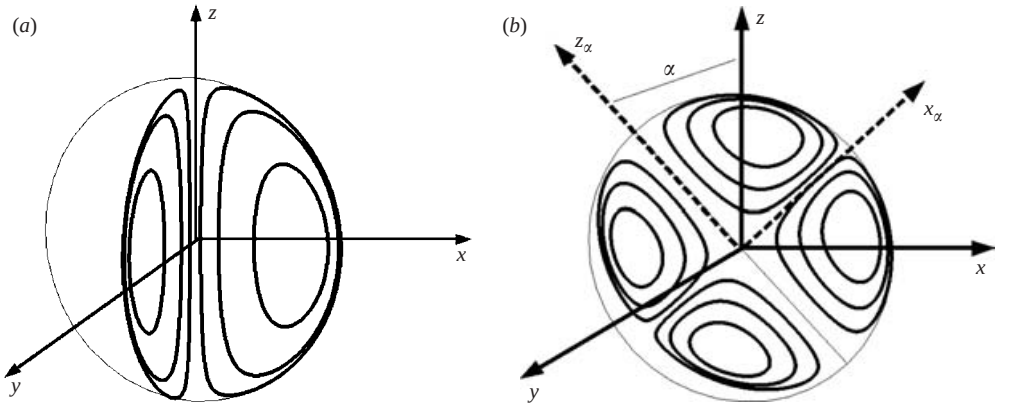

FIGURE 1. (*a*) Hadamard–Rybczynski and (*b*) Taylor flow inside a drop. Note the Taylor circulation is rotated about the *y*-axis by an angle α relative to the Hadamard–Rybczynski circulation.

superposition there is a plane of symmetry. Particle trajectories approaching this plane have to either cross the SUF or change direction and return along the path on which they came. Trajectories that change direction may repeat this process indefinitely, leading to the appearance of KAM surfaces, or adiabatic invariants, which are barriers to efficient mixing. Grigoriev (2005) offers solutions to breaking the symmetric regions by introducing time dependence in a drop where the circulation is a combination of three flow fields. Ward & Homsy (2001, 2003) also showed theoretically and experimentally that time dependence in an otherwise axisymmetric flow can destroy symmetries.

Although chaotic streamlines inside drops have been predicted in the works cited above, none of the means of producing such flows is particularly simple. Here we consider the creation of chaotic flows by electrical stresses which requires no mechanical forcing of an external flow. In addition, in spite of the relatively large number of theoretical studies, there are no experiments that test important aspects of these theories. Conducting such experiments is one of the main objectives of this work.

In § 2, we describe the theoretical model and expressions for the circulation produced inside a translating drop in the presence of a spatially uniform electric field. Section 2.1 contains the background theory and § 2.2, our numerical method. We then determine the qualitative degree of mixing from Poincaré mapping in § 2.3 and in § 2.4 we quantitatively estimate the largest volume sampled by a single streamline. Then we solve for the quantitative rate of mixing by calculating the largest Lyapunov exponent in § 2.5. In § 3 we discuss the experimental technique and procedure. In § 4 we analyse the experimental data and make some comparisons between them and the theoretical predictions.

2. Theory

2.1. *Background and scaling*

Consider a drop of radius a translating in the presence of a spatially uniform steady electric field $\boldsymbol{E}$. The relevant physical parameters include the resistivities $1/\sigma_i$, the electric permittivities $\kappa_0\kappa_i$ (where $\kappa_0 = 8.85 \times 10^{-12}$ in MKS units is the electric permittivity constant), the absolute viscosities μ_i and the densities ρ_i, where subscripts

1, 2 will denote the continuous and disperse phases respectively. The flow depends on the dimensionless property ratios $X = \sigma_2/\sigma_1$, $S = \kappa_1/\kappa_2$ and $\lambda = \mu_2/\mu_1$. The drop settles with characteristic velocity U and the electrically driven circulation has characteristic speed V, which is proportional to the square of the electric field $|E|^2$. The capillary numbers $Ca_E = V\mu/\gamma$ and $Ca_U = U\mu/\gamma$ are assumed to be small, with the consequence that the drop remains spherical. We further assume that the Reynolds number is small, i.e. $Re = Ua/4\nu(1+\lambda) \ll 1$, and analogously that charge convection is negligible, i.e. $Pe = (|E|\kappa\kappa_0)^2/\mu\sigma \ll 1$. The dimensionless velocity $W = 4V(1+\lambda)/U$ represents the relative strength of the Taylor to the Hadamard–Rybczynski circulations. The electric field is tilted by an angle α relative to the drop settling motion as shown in figure 1(*b*). The advection equations in Cartesian coordinates are:

$$\begin{pmatrix}\dot{x}\\ \dot{y}\\ \dot{z}\end{pmatrix} = \begin{pmatrix}2xz\\ 2yz\\ -4x^2-4y^2-2z^2+2\end{pmatrix} + W\begin{pmatrix}\cos\alpha & 0 & \sin\alpha\\ 0 & 1 & 0\\ -\sin\alpha & 0 & \cos\alpha\end{pmatrix}\begin{pmatrix}x_\alpha^3 + x_\alpha y^2 + 3x_\alpha z_\alpha^2 - x_\alpha\\ y x_\alpha^2 + y^3 + 3y z_\alpha^2 - y\\ 2z_\alpha - 4x_\alpha^2 z_\alpha - 4z_\alpha y^2 - 2z_\alpha^3\end{pmatrix} \tag{2.1}$$

where

$$\left.\begin{aligned} x_\alpha &= x\cos\alpha - z\sin\alpha,\\ z_\alpha &= z\cos\alpha + x\sin\alpha.\end{aligned}\right\} \tag{2.2}$$

Here the overdot denotes a time derivative, and x_α and z_α are the coordinates for the tilted Taylor circulation relative to the settling drop coordinates x and z respectively. Since the y-coordinate is invariant under the rotation there is a plane of symmetry at $y = 0$. This is also reflected in the Jacobian term in equation (2.1), appearing after the dimensionless velocity W. Another symmetry plane occurs at $x = 0$ for the particular case of $\alpha = \pi/2$, which divides the circulation into four symmetric cells. The problem is therefore governed by two parameters, the tilt angle α and the dimensionless velocity $W = 4V(1+\lambda)/U$. We are interested in the mechanics of chaotic advection and the parametric dependence of the mixing that results.

2.2. *Particle trajectories*

Lagrangian particle trajectories are used to investigate features of the mixing. Depending upon the parameters W and α, and the initial position $\boldsymbol{x}(0)$, a Langrangian particle may travel along a trajectory that may fill the drop interior. The advection equations are numerically advanced in time using an implicit Runge–Kutta method and converges to machine precision with Newton–Raphson iterations.

Figure 2(*a*) shows an example of a trajectory for $W = 2$, $\alpha = \pi/4$ and $\boldsymbol{x}(0) = (0.3, 0.4, -0.3)$ in three-dimensional perspective, which suggests its chaotic nature. Further insight is gained from figure 2(*b*, *c*) which shows two projections of another chaotic trajectory where the tilt angle is $\alpha = \pi/10$, $W = 2$ and $\boldsymbol{x}(0) = (0.3, 0.6, 0.4)$. In this case the trajectory winds around the drop interior and the location of the SUF (for $\alpha = 0$) is clearly visible. As mentioned, crossing the SUF produces chaotic trajectories.

The next sequence of images, figure 3, illustrates two events that are the main focus of this paper, one event leading to mixing and the other not. Figure 3(*a*, *b*) shows a trajectory as it rotates in the lower section of the drop then moves into the top portion.

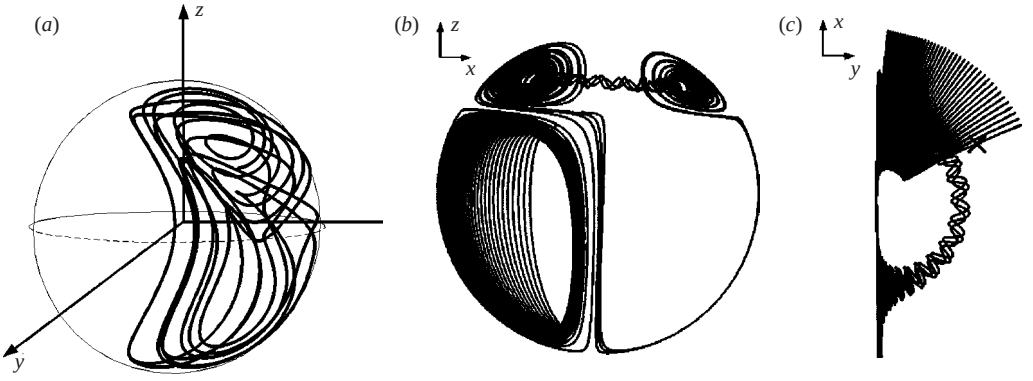

FIGURE 2. (*a*) Numerical simulation of a particle trajectory for the combined flow field for $W = 2$, $\alpha = \pi/4$ and $\boldsymbol{x}(0) = (0.3, 0.4, -0.3)$. (b, c) Numerical simulation of a particle trajectory for the combined flow field for $W = 2$, $\alpha = \pi/10$ and $\boldsymbol{x}(0) = (0.3, 0.6, 0.4)$.

The second sequence, figure 3(c, d) shows a particle trajectory that approaches the plane of symmetry at $y = 0$. As it does so, it changes its azimuthal direction then wraps around inside its initial path leading to trajectories that, by repeating the process, are confined to a surface. The confined region is a KAM surface which is a barrier to efficient mixing. We expect to see both of these features in the experiments.

2.3. *Poincaré maps*

Poincaré maps were constructed by launching a Langrangian particle and plotting its position as it crosses a particular plane, with a map typically containing 10^4 crossings. While for axisymmetric flows a single Poincaré map describes the ordered and chaotic regions, in three-dimensional they depend on the choice of plane. We choose $x = 0$ and $x_\alpha = 0$, parallel to the settling velocity and to the electric field, respectively.

Figure 4 shows Poincaré maps for $W = 2, 4, 10$ and $\alpha = 3\pi/50$, $9\pi/50$ and $2\pi/5$ in the $x = 0$ plane. Treating $W = 2$ and $\alpha = 3\pi/50$ (figure 4*a*) as a reference case, as we increase the tilt angle more of the domain is sampled by the particle. This trend is also seen for $W = 4$. For $W = 10$ however, figure 4$(g$–$i)$ shows that as we increase the tile angle there is little change in the area covered, suggesting there is an optimal value of W for maximum mixing. If instead we investigate trends for increasing W for fixed α, we see that less of the area is covered as W increases. So the general trends are an increase in mixing with increasing angle and a value of W for which we observe maximum mixing.

In all of the examples shown so far particles sample a relatively large region. This is not always the case. These results are sensitive to initial condition and the flow possesses regions that are separate and contain different dynamics. Figure 5 shows a Poincaré map for the section $x_\alpha = 0$ with $W = 2$ and $\alpha = \pi/3$ for two different initial conditions, $\boldsymbol{x}_1(0) = (-0.6, 0.4, -0.2)$ and $\boldsymbol{x}_2(0) = (0.6, 0.4, -0.2)$, superimposed on one plot. For one initial condition, $\boldsymbol{x}_2(0)$, the trajectory fills up most of the domain while that for the other initial condition $\boldsymbol{x}_1(0)$ is confined to a KAM surface and appears not to mix at all. This happens, in part, because after a particle trajectory approaches the symmetry plane at $y = 0$ there are only two possibilities: (i) cross the SUF and mix in the upper portion of the drop or (ii) stay in the lower section of the drop and follow the direction from which it came, thus encountering the same symmetry plane. At first glance we should consider these KAM surface as ordered regions since the motion is confined to a surface, but Poincaré maps are only one

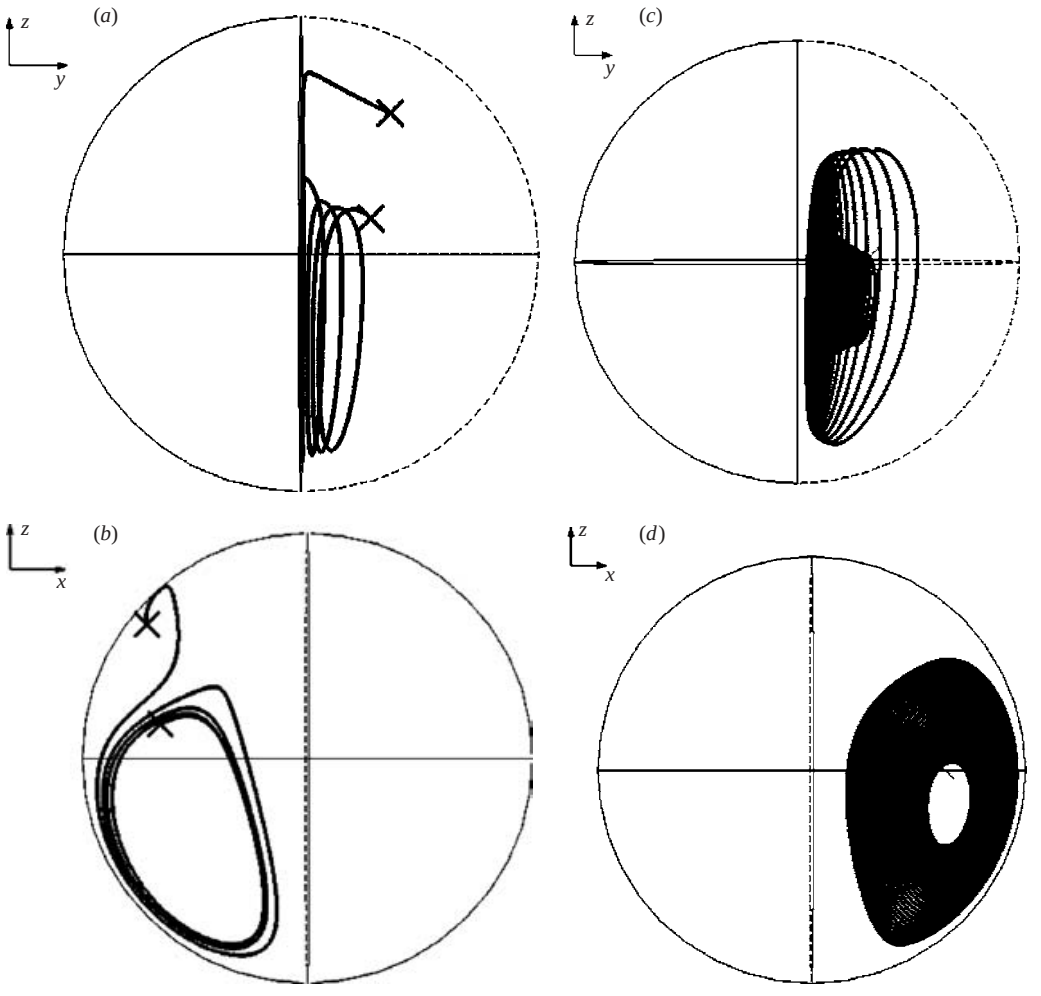

FIGURE 3. (a, b) A particle trajectory as it crosses the separatrix of the Taylor circulation. The $\times$ mark the initial and final positions. (c, d) A particle trajectory that approaches the symmetry plane then changes direction. This trajectory leads to KAM surfaces which are barriers to mixing.

measure of chaotic advection. In the next section we study the largest volume sampled by a single streamline followed by mixing rate estimates.

2.4. *Mixed volume estimates*

As shown qualitatively in the previous section a single streamline may partially fill the drop volume depending on its initial position. In this section we calculate the largest volume that a single streamline can sample as a function of the parameters $1 \leqslant W \leqslant 10$ and $0 \leqslant \alpha \leqslant \pi/2$ (the velocity field and hence the mixed volume is symmetric about $\pi/2$). The technique to estimate the largest volume is as follows: first an initial condition is chosen and then a box is drawn around each point that a particle samples for a given set of parameters W and α. The boxes are tallied, each box counted only once, and this number is divided by the total number of boxes that can fit within a single drop. The calculation is performed for several initial conditions to ensure that the largest volume sampled is recorded, which in practice requires that the

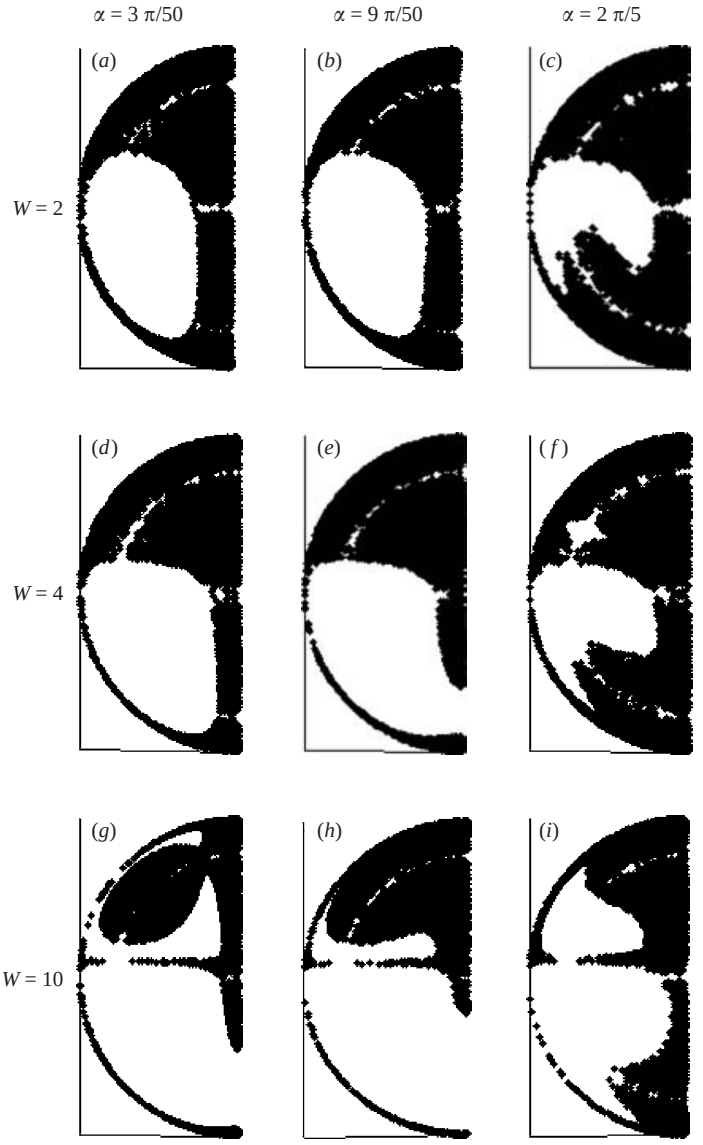

FIGURE 4. Poincaré maps in the $x = 0$ plane for various parameters.

trajectory crosses the SUF. It should be noted that the largest mixed volume possible for a single streamline is half of the total drop volume due to the symmetry plane at $y = 0$. At $\alpha = \pi/2$ there is another plane of symmetry at $x = 0$ so the maximum possible mixed volume fraction at that value is 0.25. Extensive calculations of this type were done.

Figure 6 shows the estimates of the mixed volume versus tilt angle α for $W = 1, 1.5, 2, 4, 10$. The general trend is an increase and then decrease in mixed volume with α for any given W. This can be rationalized by the fact that $\alpha = 0$ represents an integrable flow and at $\alpha = \pi/2$ another symmetry plane is introduced so the maximum mixed volume decreases by 50 %. A cross-plot of mixed volume versus W for fixed α shows a maximum at intermediate W. This may be rationalized by noting

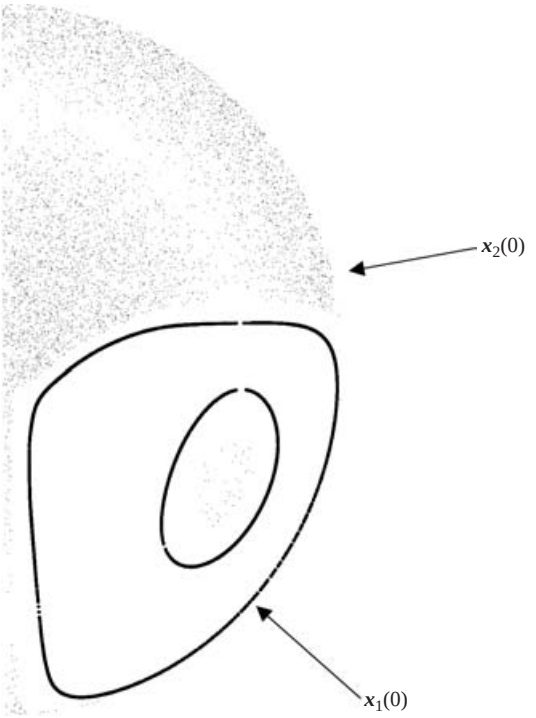

FIGURE 5. Poincaré maps in the $x_\alpha = 0$ plane for two initial conditions $\boldsymbol{x}_1(0) = (-0.6, 0.4, -0.2)$ and $\boldsymbol{x}_2(0) = (0.6, 0.4, -0.2)$ superimposed on one plot. The second initial condition fills most of the domain while the first is confined to a KAM surface.

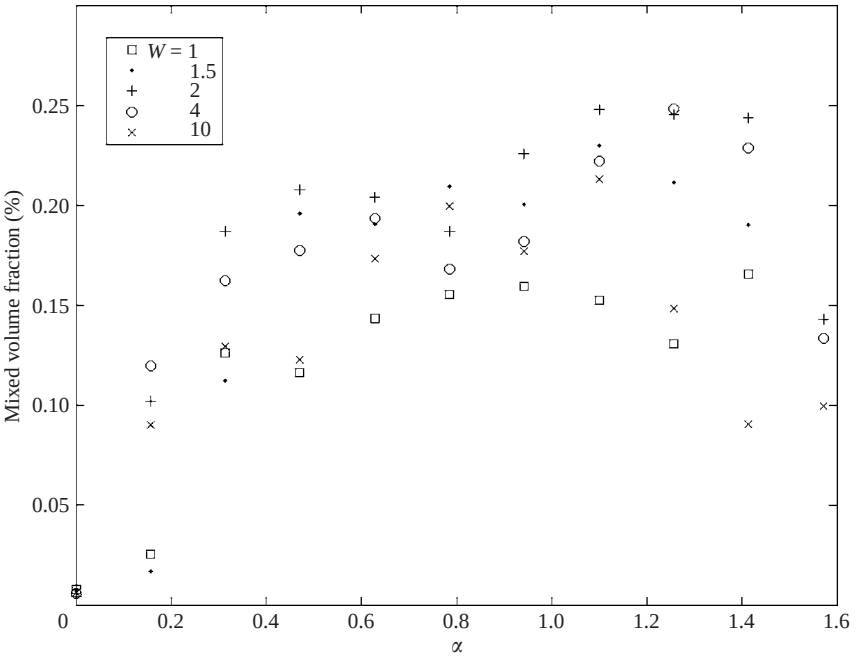

FIGURE 6. Percentage of mixed volume vs. tilt angle α for $W = 1, 1.5, 2, 4, 10$.

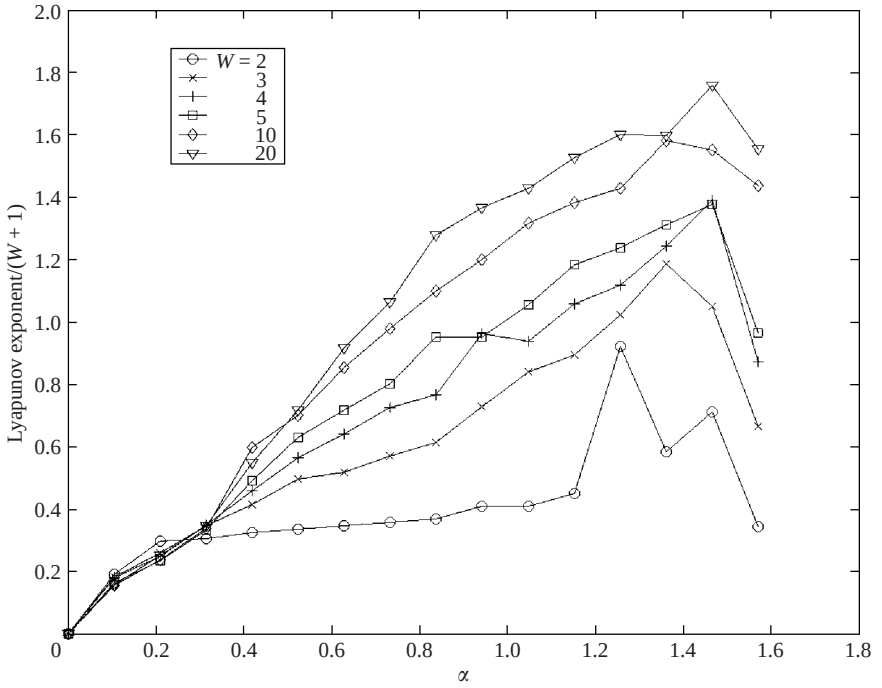

FIGURE 7. Scaled Lyapunov exponent vs. electric field tilt angle α for $W = 2, 3, 4, 5, 10, 20$.

that both $W = 0$ and $W \to \infty$ are integrable flows, with similar conclusions regarding the existence of an optimal W. While the data may be slightly noisy, it appears that the optimal value is near $W = 2$, although the cross-plot is flat for small α and there is a range of α where the maximum shifts to slightly lower W. Focusing on the $W = 2$ data as representative of the general locus of optimal W, there appear to be two local extrema in α, located near 0.4 and 1.2, respectively, with the second of these generally resulting in a larger mixed volume. The global maximum, which again appears to be relatively flat in W, occurs for $1.0 < \alpha < 1.4$, and $2 < W < 4$, and results in mixed volumes near 25%.

The next section considers other aspects of the dynamics within the chaotic region by calculating the rate of mixing via the largest Lyapunov exponent.

2.5. *Lyapunov exponents*

Lyapunov exponents provide a measure of the average rate of mixing along a chaotic trajectory. We should note that calculating volume-preserving Lyapunov exponents was not originally developed in the context of bounded flows but the technique was used by Bajer *et al.* (1990) to analyse the rate of trajectory separation for their flow. In general a value greater than zero means exponential divergence of the trajectories of two initially close particles, which also is a sign of chaotic advection. The largest exponent is calculated as

$$\xi = \lim_{n\to\infty} \frac{1}{n\Delta t} \sum_{i=1}^{n} \ln |d_i|, \tag{2.3}$$

where $\boldsymbol{d}_i$ is the particle displacement, and Δt is a uniform time interval. The Lyapunov exponent versus tilt angle $0 \leqslant \alpha \geqslant \pi/2$ for various values of W is shown in figure 7. The Lyapunov exponents are all calculated along trajectories which

Fluid	Density ($\mathrm{kg\,m^{-3}}$)	Viscosity ($\mathrm{kg\,m^{-1}\,s^{-1}}$)	Dieletric constant	Conductivity $(\Omega\,\mathrm{m})^{-1}$
Castor oil	957	0.749	2.75	$< 10^{-11}$
Silicone oil	963	0.0597	4.45	$< 10^{-13}$

TABLE 1. Table of physical properties.

sample the complete domain unless otherwise stated. The exponents are scaled by the dimensionless velocity parameter $1 + W$, similar to the scaling suggested previously (Ward & Homsy 2001). As shown in figure 7 the plots of the Lyapunov exponents are all similar in shape and are nearly identical for small tilt angle $\alpha < 0.4$. There is also a maximum for each value of W that occurs around the same range of tilt angles $\alpha \sim 1.3$–1.4. Although there is no *a priori* reason to expect the Lyapunov exponents to be continuous in the parameters, one can see from figure 7 that there is a general trend. This trend is a linear increase and the decrease near $\alpha = \pi/2$ is due to the confinement from the introduction of a second plane of symmetry.

Next we calculate Lyapunov exponents for $W = 2$ and $\alpha = \pi/3$ where two trajectories (see figure 5) displayed different dynamics as observed on the Poincaré maps. For the initial condition $\boldsymbol{x}_1(0) = (-0.6, 0.4, -0.2)$, $\xi_1 = 1.2$, while for the other initial condition $\boldsymbol{x}_2(0) = (0.6, 0.4, -0.2)$, $\xi_2 = 0.5$. The initial condition $\boldsymbol{x}_2(0)$ yields chaotic trajectories that cover most of the domain on the Poincaré maps but has a lower rate of mixing than the other, i.e. $\xi_1 > \xi_2$. While it may seem unusual that a three-dimensional KAM surface has a finite Lyapunov exponent, the explanation is that the Lyapunov exponent is a measure of transient behaviour. For example, Lyapunov exponents for $\alpha = 0$ are all zero over the given time interval $n \sim O(10^6)$ and $\Delta t \sim O(10^{-3})$ but exhibit finite values over short intervals $n\Delta t \sim O(1)$. As $n\Delta t \to \infty$ the Lyapunov exponent must go to zero for a bounded flow since $|d_i|$ is always finite. Therefore the Lyapunov exponent for the three-dimensional KAM surface which samples a larger volume than its two-dimensional counterpart, $\alpha = 0$, asymptotes to zero before a trajectory that crosses the separatrix which samples more of the volume. A more complete study of this behaviour requires much longer computational time and is outside the scope of this paper.

So far we have shown predictions of chaotic particle trajectories and identified the phenomenon of crossing the SUF as the main mechanism leading to chaotic advection. On the other hand we identified trajectories that do not cross the SUF, resulting in KAM surfaces. We validate our predictions in the next section by providing experimental evidence of these two features.

3. Experiments

We conduct experiments to test the predictions of the previous section. In particular we are interested in observing the key features of this flow, discussed in detail in § 2.2: the presence of a symmetry plane and trajectories that cross the SUF.

3.1. *Experimental setup*

The experiments are performed with drops of silicone oil in a castor oil continuous phase and table 1 gives the accepted values of both the physical and electrical properties of both fluids (Taylor 1966; Vizika & Saville 1992; Saville 1997). In terms of dimensionless parameters: $S = 0.62$, $X \sim 10^{-2}$ and $\lambda = 0.08$. Since

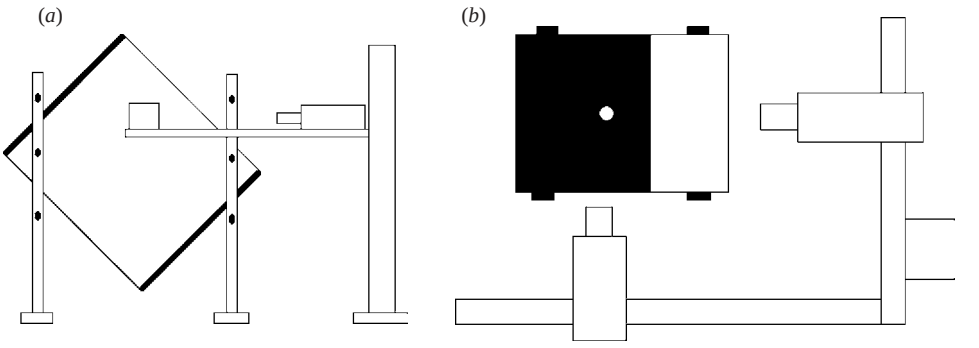

FIGURE 8. Schematic (*a*) side and (*b*) top view of the experimental setup.

$SX - 1 < 0$ we will produce the desired Taylor circulation in the predicted direction. A slight density mismatch produces a finite settling velocity yielding the Hadamard–Rybczynski circulation. An acrylic tank with inner dimensions 26 cm × 26 cm × 26 cm is filled with castor oil. The tank is supported by a plastic stand held in place by screws tapped in the tank walls. Holes are drilled in the legs of the stand in increments so the tank angle can be adjusted. The top and the bottom of the tank are fitted with copper electrodes, with a small hole in the top electrode to insert the silicone oil drops. The voltage potential is supplied by a Spellman high-voltage unit capable of up to 30 kV. Two tracks are joined at a right angle and mounted on a translational stage with a programmable Pulnix CCD camera on each track. The cameras are positioned as close as possible to normal with the tank walls: this alignment will affect the location of the symmetry plane when visualized by particle tracking. The camera exposure time is externally controlled. Light sources are positioned behind the tank, directly in front of the CCD cameras. A schematic of the setup is shown in figure 8.

3.2. *Operating conditions, procedure and visualization technique*

The drops are approximately 5 mm in diameter and translate with a speed of about 0.16 mm s^{-1}. The indices of refraction are nearly the same for the two fluids and the acrylic tank, which minimizes optical distortion. The distance between the electrodes is 26 cm; therefore one expects to record data for at most 26 minutes at small tilt angles. The frame rate of the CCD cameras is set to 1 frame s^{-1} resulting in as many as 1500 frames per run. The maximum voltage we can achieve is 30 kV. For the 26 cm tank this results in a maximum dimensionless velocity value of $W = 10$. However, due to significant drop deformation at high voltages we limit the maximum dimensionless velocity to $W \sim 4$. Also limited are the tank tilt angles because of the ability to clearly view the drop interior through the murky castor oil. By trial and error we determine the maximum tilt angle we can achieve to be $\alpha = 0.31$. Accordingly, we chose $W = 2.1$–4.4 and $\alpha = 0.19$–0.31 as the range of parameters.

The silicone oil drops are seeded with neutrally buoyant glass particles $O(10\,\mu\text{m})$ to visualize particle trajectories. Each drop is seeded with only a few particles so individual particles can be unambiguously identified and tracked. The particle tracking is performed by an algorithm described below. The drops are inserted into the hole in the top electrode and settle for a few minutes before they are in position to be viewed. Once in position the high-voltage unit is turned on and the cameras are positioned. The translational stage then is set to the speed of the falling drop and the recording begins. The images are saved to a computer for analysis.

The recorded sequence of images is analysed by tracking the position of the glass particles inside the settling drop. The raw data images are saved in bitmap format, which is a matrix representation of the actual image. The translational stage does not exactly match the settling speed so the orthogonal images are first registered with the location of the drop in the first image. Then a particle is selected from the first image and its position, in that view, is recorded. Images of this particle from the left and right views are matched by its initial z location. A small box is drawn around the particle and this box is placed in the next image. If the location of the particle is in the box on the next frame, its position is recorded and the process is repeated for all the frames. This technique is possible because the particles are moving slowly. The particle position data are scaled by the drop size and the position is translated so that the centre of the drop is $\boldsymbol{x} = (0, 0, 0)$. The results from the left and right views are combined and the three-dimensional trajectory is recreated.

4. Experimental results and discussion

4.1. *Crossing the separatrix of the unperturbed flow (SUF)*

In this section we show experimental results of particle trajectories that cross the SUF of the combined Hadamard–Rybczynski and Taylor circulations. There are four combinations of parameters that we analyse: two dimensionless velocities $W = 2.1$, 4.4 and two tilt angles $\alpha = 0.19$, 0.31, with several trajectories analysed from each set of parameters.

Figures 9(a) and 9(b) are plots in the (y, z)- and (x, z)-plane (positive x points to the rear of the drop) showing the path of a single particle for the reference case of $W = 2.1$ and $\alpha = 0.19$. The electric field tilt is oriented as shown in figure 1, i.e. about the y-axis. Each point represents the particle position in 1 s intervals. The particle first follows a trajectory resembling the lower portion of the stacked vortex structure of the Taylor circulation. It does so for a few minutes, then after 600 s it travels to the top of the drop and starts to rotate in the opposite direction, evidence that it has crossed the SUF.

Figure 9(c, d) shows a trajectory crossing the SUF with $W = 2.1$ and $\alpha = 0.31$, i.e. for a larger angle than the reference case. The trajectory crosses the SUF near the equator, i.e. in a lower region of the drop than in figure 9(a, b). A plausible explanation is that as the electric field tilt increases the tilt of the separatrix from the Taylor circulation also increases. Hence, as the tilt increases, crossing the SUF should occur at a lower value at the rear along the z-axis.

Figure 10(a–d) shows trajectories for $W = 4.4$ and $\alpha = 0.19$, i.e. for higher W than the reference case in figure 9(a, b). In figure 10(a, b) the trajectory winds around a path that is similar to a closed trajectory from the Taylor circulation and then approaches the symmetry plane. After this it winds around toward the rear of the drop and then crosses the SUF. The crossing appears to start a little below the equator. We can explain this if we recall that as we increase the dimensionless velocity W with $\alpha = 0$ the separatrix from the Taylor circulation moves closer to the equator, its axial distance from the equator being given by $1/W$. A similar dependence is present in the three-dimensional case; as we increase W the separatrix moves close to the equator, the equator being the location of the tilted separatrix from the Taylor circulation in the absence of the drop translation. This effect is further shown in figure 10(c, d) where the crossing occurs near the front of the drop. The particle first winds around a trajectory resembling a closed streamline from the combined Hadamard–Rybczynski and Taylor circulations with $\alpha = 0$ and then travels into the top portion of the drop.

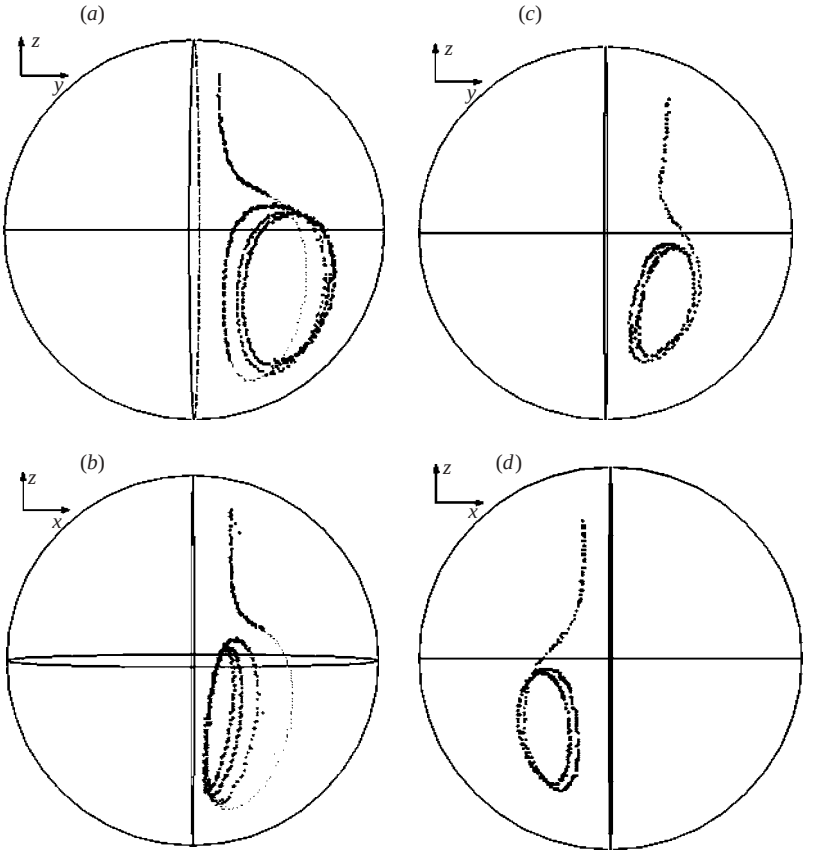

FIGURE 9. Particle trajectory for (a, b) $W = 2.1$ and $\alpha = 0.19$, (c, d) $W = 2.1$ and $\alpha = 0.31$.

After the particle is well into the top half, it begins to change swirling direction, a clear indication that it has crossed the SUF.

Figure 10(e, f) with $W = 4.4$ and $\alpha = 0.31$ shows another crossing of the SUF. The rotation in the lower half of the drop resembles a closed streamline from the combined circulation. But this time the rate of drift is stretched in the azimuthal direction and is larger than in the previous cases. Once again the crossing occurs near the equator but closer to the pole than in the earlier results above. This follows from the previous explanation that as we increase W the SUF moves closer to the equator. Analogously, when the tilt is increased the separatrix penetrates more of the lower portion of the drop. This means that particles are more likely to cross the SUF from below the equator near the rear of the drop.

4.2. *Symmetry plane*

Figure 11(a, b) shows two particle trajectories labelled 1 and 2 with $W = 2.1$ and $\alpha = 0.19$. Trajectory 1 lies adjacent to the symmetry plane (recall that the CCD cameras are not exactly normal to the tank walls so the symmetry plane does lie exactly on the horizontal axis). It winds around in an increasing spiral that resembles a closed streamline pattern from the Taylor circulation. After some time the trajectory leaves the symmetry plane and returns to the $y < 0$ hemisphere. This is similar to figure 3(c, d) where we plot a trajectory as it leaves the symmetry plane and recirculates. Trajectory 2 is from the same drop and shows a tighter spiral

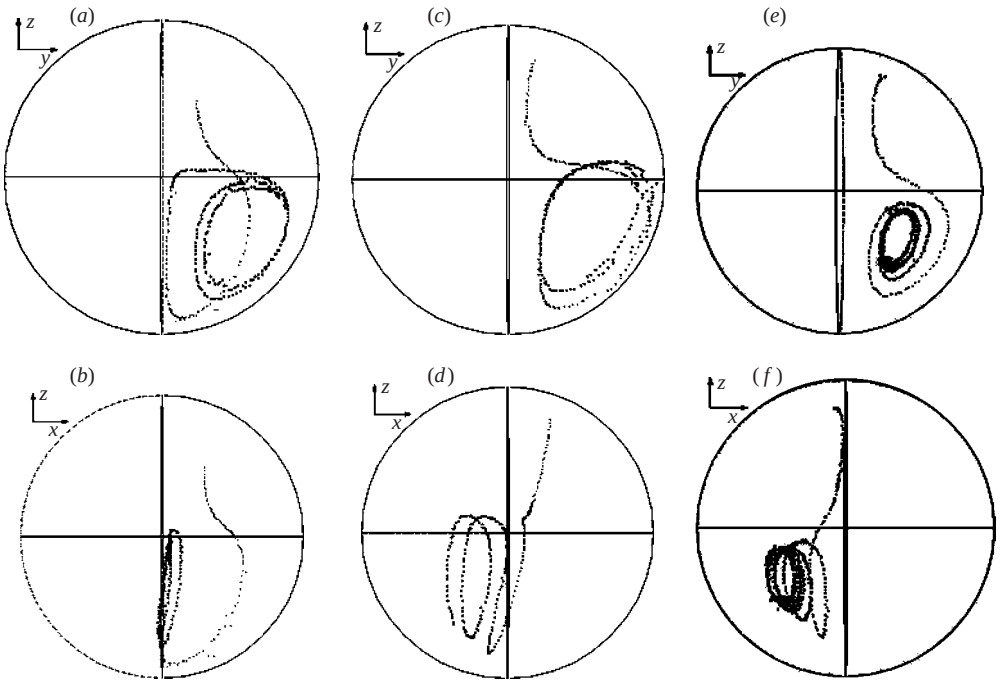

FIGURE 10. Particle trajectory for (a, b) $W = 4.4$ and $\alpha = 0.19$, (c, d) $W = 4.4$ and $\alpha = 0.19$, (e, f) $W = 4.4$ and $\alpha = 0.31$.

trajectory travelling toward the symmetry plane where trajectory 1 is leaving. Both these trajectories are in the $y < 0$ hemisphere and both in the lower portion of the drop but moving in opposite directions. This is evidence that the two trajectories are portions of a KAM surface.

Figure 11(c, d) also shows two particle trajectories but on opposite sides of the symmetry plane. Trajectories 1 and 2 start nearly opposite each other and travel along similar paths. This suggest that there is symmetry in the flow between the two halves of the drop.

5. Summary and conclusion

We have presented theoretical and experimental results for mixing inside a settling drop with a steady tilted electric field. The theoretical model is based on a quasi-static assumption for the electric field and neglects charge convection. The parameters are the electric field tilt angle α, relative to the settling motion, and the dimensionless velocity W. Taking the tilt angle as the perturbing variable, crossing the separatrix of the undisturbed flow (SUF) is identified as a feature of chaotic advection in the combined three-dimensional flow. As trajectories cross the SUF they change rotational direction, and the exchange of fluid between these regions leads to mixing. Particles do not always cross the SUF, as some particles travel along paths that are confined to a KAM surface. The theory predicts that it should be possible to produce three-dimensional steady chaotic flows without using mechanical means; rather we manipulate electrical stresses to produce the desired results.

The numerical results suggest that there is an optimal range of parameters. In particular there is an optimal electric field value, or dimensionless velocity W,

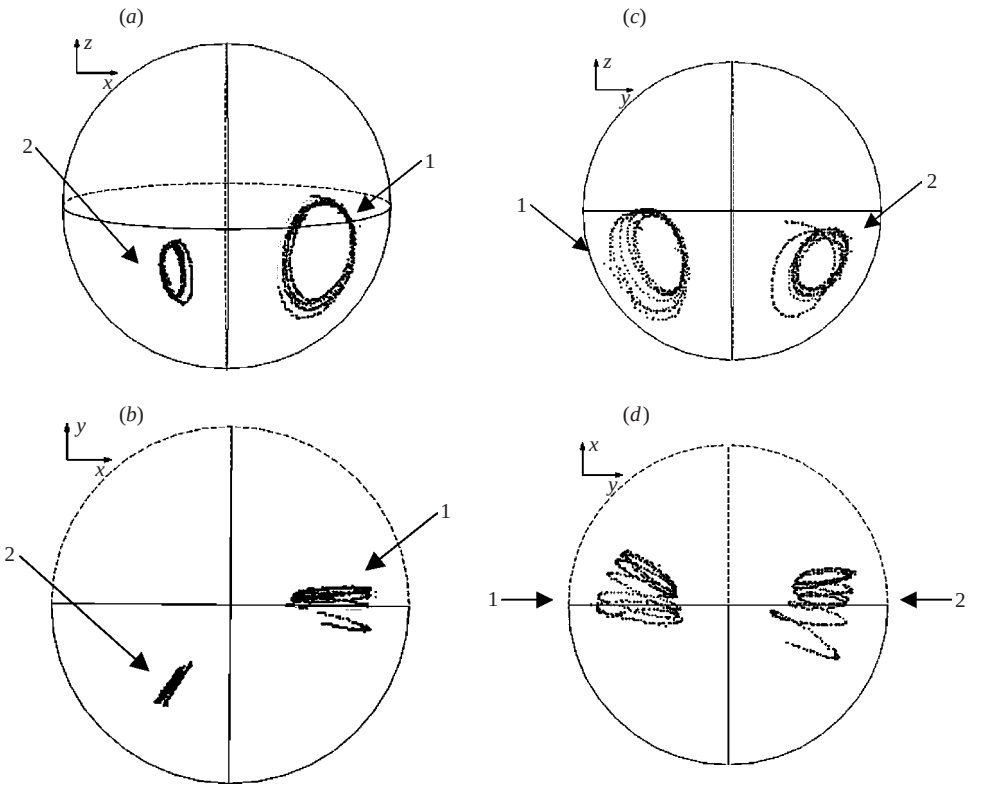

FIGURE 11. Visualization of two particle trajectories for (a, b) $W = 2.1$ and $\alpha = 0.19$. Note that trajectory 1 approaches the symmetry plane then changes direction. (c, d) Two particle trajectories for $W = 4.4$ and $\alpha = 0.31$. Note the two trajectories are on opposite halves of the drop and have similar shape.

according to the Poincaré maps, and an optimal electric field tilt angle according to the Lyapunov exponents. These are determined by extensive computation of the percentage of the drop that is mixed.

Experiments are carried out using a castor oil continuous phase and a silicone oil dispersed phase. The drops are seeded with a few passive glass particles so each individual particle can be tracked. We use orthogonal view CCD cameras to determine the existence of three-dimensional chaotic trajectories.

The experiments and theoretical predictions agree well for the parameter values studied. In particular we show trajectories crossing the SUF and examine the parametric dependence of this event and connect it with our theoretical predictions. We also show evidence of the predicted symmetry through a trajectory that approaches the symmetry plane then changes direction.

This work was supported by the Office of Basic Energy Sciences, U.S. Department of Energy and by the Microgravity Science Division of NASA.

REFERENCES

BAJER, K. & MOFFATT, H. K. 1990 On a class of steady confined Stokes flows with chaotic streamlines. *J. Fluid Mech.* **212**, 337–363.

Bajer, K. & Moffatt, H. K. 1992 Chaos associated with fluid inertia. In *Topological Aspects of the Dynamics of Fluids and Plasmas* (ed. Moffatt, Zavlavsky, Comte & Tabor), pp. 517–534. Kluwer.

Bajer, K., Moffatt, H. K. & Nex, F. H. 1990 Steady confined Stokes flows with chaotic streamlines. In *Topological Fluid Dynamics* (ed. H. K. Moffatt & A. Tsinober), pp. 459–466. Cambridge University Press.

Bryden, M. D. & Brenner, H. 1999 Mass-transfer enhancement via chaotic laminar flow within a droplet. *J. Fluid Mech.* **379**, 319–331.

Cary, J. R., Escande, D. F. & Tennyson, J. L. 1986 Adiabatic-invariant change due to separatrix crossing. *Phys. Rev.* A **34**, 4256–4275.

Chang, L. S., Carleson, T. E. & Berg, J. C. 1981 Heat and mass transfer to a translating drop in an electric field. *Intl J. Heat Mass Transfer* **2512**, 1023–1030.

Grigoriev, R. O. 2005 Chaotic mixing in thermocapillary-driven microdroplets. *Phys. Fluids* **17**, 033601.

Kronig, R. & Brink, J. C. 1949 On the theory of extraction from falling droplets. *Appl. Sci. Res.* A **2**, 142–154.

Kroujiline, D. & Stone, H. A. 1999 Chaotic streamlines in a steady bounded three-dimensional Stokes flow. *Physica* D **130**, 105–132.

Lichtenburg, A. J. & Lieberman, M. A. 1992 *Regular and Chaotic Dynamics*. Springer.

Neishtadt, A. 1984 The separation of motions in systems with rapidly rotating phase. *J. Appl. Math. Mech.* **48**, 133–139.

Neishtadt, A. I., Vainshtein, D. L. & Vasiliev, A. A. 1998 Chaotic advection in a cubic Stokes flow. *Physica* D **111**, 227–242.

Saville, D. A. 1997 Electrohydrodynamics: The Taylor-Melcher Leaky Dielectric Model. *Annu. Rev. Fluid Mech.* **29**, 27–64.

Stone, H. A., Nadim, A. & Strogatz, S. H. 1991 Chaotic streamlines inside drops immersed in steady Stokes flows. *J. Fluid Mech.* **232**, 629–646.

Stone, Z. B. & Stone, H. A. 2005 Imaging and quantifying mixing in a model droplet micromixer. *Phys. Fluids* **17**, 063103.

Taylor, G. I. 1966 Studies in Electrohydrodynamics I. The circulation produced in a drop by an electric field. *Proc. R. Soc. Lond.* A **291**, 159–166.

Vainshtein, D. L., Vasiliev, A. A. & Neishtadt, A. I. 1996 Changes in the adiabatic invariant and streamline chaos in confined incompressible Stokes flow. *Chaos* **6**, 67–77.

Vizika, O. & Saville, D. A. 1992 The electrohydrodynamic deformation of drops suspended in liquids in steady and oscillatory fields. *J. Fluid Mech.* **239**, 1–21.

Ward, T. & Homsy, G. M. 2001 Electrohydrodynamically driven chaotic mixing in a translating drop. *Phys. Fluids* **13**, 3521–3525.

Ward, T. & Homsy, G. M. 2003 Electrohydrodynamically driven chaotic mixing in a translating drop Part II: Experiments. *Phys. Fluids* **15**, 2987–2994.